HHS Public Access

Author manuscript

Gene Ther. Author manuscript; available in PMC 2015 April 01.

Published in final edited form as:

Gene Ther. 2014 October ; 21(10): 903–912. doi:10.1038/gt.2014.70.

Re-engineered p53 Activates Apoptosis In Vivo and Causes Primary Tumor Regression in A Dominant Negative Breast Cancer Xenograft Model

Abood Okal[1], **Karina J. Matissek**[1,2], **Stephan J. Matissek**[3], **Robert Price**[1], **Mohamed E. Salama**[4], **Margit Maria Janát-Amsbury**[1,5,6], and **Carol S. Lim**[1,6,*]

[1]Department of Pharmaceutics and Pharmaceutical Chemistry, University of Utah, Utah, USA

[2]Department of Pharmaceutics and Biopharmacy, Philipps-Universität, Marburg, G ermany

[3]Faculty of Biotechnology, Biberach University of Applied Sciences, Germany

[4]Department of Pathology, University of Utah, Utah, USA

[5]Division of Gynecologic Oncology, Department of Obstetrics and Gynecology, University of Utah, Utah, USA

[6]Huntsman Cancer Institute, University of Utah, Utah, USA

Abstract

Inactivation of p53 pathway is reported in more than half of all human tumors and can be correlated to malignant development. Missense mutation in the DNA binding region (DBD) of p53 is the most common mechanism of p53 inactivation in cancer cells. The resulting tumor-derived p53 variants, similar to wild-type (wt) p53, retain their ability to oligomerize via the tetramerization domain (TD). Upon hetero-oligomerization, mutant p53 enforces a dominant negative effect over active wt-p53 in cancer cells. To overcome this barrier, we have previously designed a chimeric superactive p53 (p53-CC) with an alternative oligomerization domain capable of escaping transdominant inhibition by mutant p53 *in vitro*. In this report, we demonstrate the superior tumor suppressor activity of p53-CC and its ability to cause tumor regression of the MDA-MB-468 aggressive p53-dominant negative breast cancer tumor model *in vivo*. In addition, we illustrate the profound effects of the dominant negative effect of endogenous mutant p53 over wt-p53 in cancer cells. Finally, we investigate the underlying differential mechanisms of activity for p53-CC and wt-p53 delivered using viral-mediated gene therapy approach in the MDA-MB-468 tumor model.

Keywords

p53; dominant negative effect; tetramerization; MDA-MB-468; coiled-coil; breast cancer

[*]**Corresponding Author**. 30 South 2000 East, Rm 2916, Salt Lake City, UT 84112, USA, Phone: 1-801-587-9711. Fax: 1-801-585-3614. carol.lim@pharm.utah.edu.

The authors declare no conflict of interest.

INTRODUCTION

The ability of p53 to achieve tumor suppressor function depends on formation of p53 tetramers to act as a transcription factor of several target genes.[1, 2] Once activated, p53 stimulates a wide network of signals including DNA repair, cell cycle arrest, and apoptosis.[3] The significance of p53 function is highlighted by the correlation of its inactivity and malignant development. Inactivation of p53 pathway is reported in more than half of all human tumors and can be achieved via several mechanisms including nuclear exclusion and hyperactivation of MDM2, the main regulator of p53 function.[4–6] However, acquisition of missense mutations in one or both alleles of the *TP53* gene remains the most common mechanism of p53 inactivation.[7] The majority of these mutations take place in the DNA binding domain (DBD) which is responsible for p53 interaction with DNA. Although mutant p53 in cancer cells may have impaired tumor suppressor function and transcriptional activity, it retains its ability to oligomerize with other mutant or wild-type (wt) p53 via the tetramerization domain (TD).[8, 9] When mutant p53 oligomerizes with wt-p53 through hetero-oligomerization, the resulting tetramer has impaired function in most cases due to *transdominant inhibition* by mutant p53 (Figure 1). The outcome of this transdominant inhibition varies significantly based on the type of mutant p53 present in cells.[10] This phenomenon is known as the dominant negative effect of mutant p53 and gives rise to a critical barrier to utilizing wt-p53 for cancer gene therapy.[11]

Our goal was to design a new, chimeric superactive p53 with the following activity: wt-p53 like functional transcriptional activity; promotion of improved, highly potent p53-dependent apoptosis; and circumvention of the dominant negative inactivating effect of endogenous mutant p53 in cancer cells. To this end, we engineered a chimeric p53 (p53-CC) that has an alternative tetramerization domain and showed its ability to escape transdominant inhibition by mutant p53 *in vitro*.[12] The Bcr oligomerization domain is a 72 amino acid coiled-coil (CC) motif that serves as an alternative oligomerization domain of p53-CC to evade hetero-oligomerization with endogenous mutant p53, and hence, bypass the dominant negative effect reported in cancer cells. The CC domain itself was tested as a control previously, and was found to be non-toxic.[12] p53-CC activity was found to retain similar tumor suppressor activity compared to exogenous wt-p53 in several cancer cell lines harboring different p53 statuses (null, wt, wt mislocalized, and mutant non-dominant). Finally, we investigated potential transdominant inhibition of p53-CC and wt-p53 via co-expression of a potent dominant negative mutant p53. As hypothesized, p53-CC retained the same levels of activity regardless of the presence of transdominant mutant p53, while wt-p53 showed loss of activity.[12]

In this report, we demonstrate the superior tumor suppressor activity of p53-CC *in vitro* and *in vivo* in MDA-MB-468, an aggressive p53-dominant negative breast cancer cell line. Furthermore, we investigate the underlying differential mechanisms of activity for p53-CC and wt-p53 in the MDA-MB-468 tumor model. Our viral-mediated gene therapy approach succeeds in demonstrating the effects of the transdominant effect of endogenous mutant p53 over p53-CC and wt-p53.

RESULTS

p53-CC induces higher levels of cell death compared to wt-p53

We[12] and others[13, 14] have shown that the MDA-MB-468 human breast adenocarcinoma cell line serves as a suitable dominant negative mutant p53 model for testing the effect of p53-CC and wt-p53. The endogenous p53 in MDA-MB-468 contains the R273H point mutation, which is known to exhibit a dominant negative effect over wt-p53.[12, 14] As we have shown previously[12, 15], p53-CC is capable of inducing cell death in this as well as other cancer cell lines, regardless of endogenous p53 status. Figure 2 illustrates the superior tumor suppressor function of p53-CC over wt-p53 in a 7-AAD viability assay which stains apoptotic and necrotic cells[16, 17] (compare Figure 2A vs 2B). Wt-p53 activity is not significantly different from that achieved by the negative control Ad-ZsGreen1 (Figure 2B vs 2C). This observation illustrates the dominant negative effect of endogenous mutant p53 over wt-p53 in cancer cells and highlights the significance of our approach to escape transdominant inhibition. These results are summarized in Figure 2D.

p53-CC caused cell death via the apoptotic pathway

Figure 2 suggests that the MDA-MB-468 cell line is a suitable tumor model to test the impact of the dominant negative effect of mutant p53 *in vivo*. Preceding animal studies, we explored the mechanism of cell death, and hypothesized that it occurs via an apoptotic pathway. Thus, three different apoptosis assays: the tetramethylrhodamine ethyl ester (TMRE) assay (analogous to the JC-1 assay), activated caspase-3/7 assay, and annexin-V staining were carried out.

Mitochondrial depolarization is measured by loss in TMRE intensity correlates with an increase in mitochondrial outer membrane permeabilization (MOMP).[18] TMRE is a cationic, cell-permeant, and fluorescent dye that rapidly accumulates in mitochondria of living cells due to the negative mitochondrial membrane potential ($\Delta\Psi m$) of intact mitochondria compared to cytosol.[19, 20] Mitochondrial depolarization results in loss of TMRE from mitochondria and a decrease in mitochondrial fluorescence intensity (FI)[7], illustrated as %MOMP induction in Figure 3A. Figure 3A demonstrates that p53-CC induced significantly higher levels of mitochondrial membrane permeabilization, a hallmark of intrinsic apoptosis, compared to wt-p53. Wt-p53 also induced mitochondrial membrane permeabilization, although not to the same extent as p53-CC. MOMP indicates that cells are transitioning to an apoptotic state.[21]

To further investigate the potential apoptotic activity of p53-CC and wt-p53, we carried out a flow cytometry-based assay to detect the levels of activated caspase-3/7 in MDA-MB-468 cells (Figure 3B). Caspase-3/7 activation is downstream from mitochondrial outer membrane permeabilization in the intrinsic apoptotic pathway and plays a central role at the execution-phase of cell apoptosis.[22–24] Figure 3B shows that cells treated with p53-CC display increased levels of active caspase-3/7 compared to those treated with wt-p53 or the negative control Ad-ZsGreen1.

Finally, annexin-V staining was performed, which measures externalization of phosphatidylserine on the cell surface of apoptotic cells specifically.[25, 26] Figure 3C shows

higher levels of annexin-V positive staining in cells treated with Ad-p53-CC compared to Ad-wt-p53; wt-p53 apoptotic activity was not significantly different from the negative control Ad-ZsGreen1. Cellular apoptosis as indicated in Figure 3C parallel the results from the 7-AAD staining in Figure 2.

To summarize, Figures 3 A, B, and C show MDA-MB-468 cells treated with Ad-p53-CC undergo significant apoptosis, validating p53-CC as a potent candidate for gene therapy. The levels of apoptosis induced by Ad-p53-CC are statistically significant compared to that of Ad-wt-p53 or Ad-ZsGreen1 in all three apoptosis assays (Figure 3) in addition to the 7-AAD assay (Figure 2).

In vivo efficacy in a dominant negative breast cancer animal model

MDA-MB-468 human breast adenocarcinoma represents an aggressive breast cancer cell line characterized as triple negative due to the absence of molecular targets including estrogen receptor, progesterone receptor, and human epidermal growth factor receptor 2.[27] In addition, MDA-MB-468 cells harbor a dominant negative mutant p53 capable of impairing the function of wt-p53.[12–14] We therefore used this cell line to induce orthotopic breast tumors in mice to compare the impact of the dominant negative effect of mutant p53 on the biological activity of p53-CC and wt-p53 in viral-mediated gene therapy. Because of the presence of the coxsackievirus and adenovirus receptor (CAR), MDA-MB-468 cells can be transfected by adenovirus.[28]

Induced in the mammary fat pad of female athymic nu/nu mice, MDA-MB-468 tumors orthotopic engraftment fosters tumorigenesis to occur in the appropriate macro- as well as microenvironment mimicking the environment of human MDA-MB-468 tumors.[29, 30] Due to this, MDA-MB-468 is a commonly used xenograft model for triple negative breast cancer.[31, 32] Tumors were allowed to grow to approximately 50 mm^3 prior to randomization of treatment groups which received intratumoral injections of Ad-p53-CC or Ad-wt-p53. The empty viral vector (Ad-ZsGreen1) served as a negative control in addition to an untreated control. Injections were made on days 0–4 and 7–11 for optimal efficacy[33] and consisted of 5.0×10^8 PFU of the viral constructs in a 50 μl volume. All procedures were performed according to established NIH guidelines and followed University of Utah Institutional Animal Care and Use Committee approved protocols.

Figure 4A shows a representative image of a tumor bearing mouse with the mammary tumor located in the right inguinal area, while Figure 4B shows images of representative excised tumors from each treatment group. The tumor size reduction expected with these treatments served as a direct measure of the tumor suppressor function of our p53 variants. As expected, the Ad-p53-CC treatment group achieved statistically significant ($p < 0.001$) reduction in mean tumor size compared to Ad-wt-p53, Ad-ZsGreen1, and untreated groups (Figure 4C). Although tumor reduction induced by Ad-wt-p53 is not statistically significant compared to the Ad-ZsGreen1 or untreated groups, Ad-wt-p53 treatment resulted in stable disease, halting tumor progression. The findings from Figure 4C reveal that p53-CC can achieve tumor *regression* of an aggressive p53-dominant negative breast cancer model *in vivo*, while wt-p53 is only capable of halting tumor progression. In addition, the excised tumors from the Ad-ZsGreen1 negative control and untreated groups appeared to be more

vascularized compared to tumors derived from the treatment groups Ad-p53-CC and Ad-wt-p53 (Figure 4B), potentially implying an additional anti-angiogenic effect of p53-CC and wt-p53 *in vivo*.

Animal body weights were regularly monitored throughout the study and no significant weight loss in animals was observed in any of the groups (Figure 4D) rendering the treatment as well as the viral carrier safe. Throughout the study, the Ad-p53-CC treatment group maintained the smallest mean tumor size compared to all other groups. Both control groups (Ad-ZsGreen1 and untreated) exhibited the largest mean tumor size compared to all other groups throughout the entire study.

Histopathological evaluation of tumor tissues and evidence for tumor suppressor activity

The tumor size reduction observed in Figure 4C indicates tumor suppressor functionality of Ad-p53-CC as well as Ad-wt-p53 *in vivo*. To verify if this activity is indeed p53-dependent, we carried out immunohistochemical staining of p21 as it is one of the best characterized bona fide p53 target genes.[34] Photomicrographs of representative sections from harvested tumor tissues from each group are displayed in Figure 5A. The left column in Figure 5A exhibits hematoxylin and eosin (H&E) staining, while the middle column represents p21 immunohistochemical staining for each group. In addition, the right column in Figure 5A shows the intratumoral expression of our gene load (i.e. p53-CC or wt-p53) as a function of the ZsGreen1 fluorescent protein co-expressed with our genes of interest. Microscopic examination of H&E staining revealed higher levels of necrosis (solid arrows, necrosis; open arrows, non-necrotic areas) in all tumors harvested from mice injected with Ad-p53-CC compared to the Ad-wt-p53, Ad-ZsGreen1, or untreated groups (Figure 5A). This implies the detected necrosis may be due to the tumor suppressor activity of p53-CC since the tumors did not reach a large enough size to develop a necrotic core, and as such the observed necrosis was due to treatment, not hypoxia.

3,3' diaminobenzidine (DAP) stains the nuclei of p21-positive cells brown, as shown in photomicrographs (middle column, Figure 5A). Unexpectedly, p21 immunohistochemistry staining revealed higher levels of p21 induction in the Ad-wt-p53 treatment group compared to the Ad-p53-CC treatment group. p21 is one of the key factors by which p53 enforces cell cycle arrest. The induction of cell cycle arrest by p21 converges with findings from Figure 4C where tumors from the Ad-wt-p53 treatment group show a halt (arrest) in tumor growth. As expected, p21 expression was not detected in the Ad-ZsGreen1 negative control or untreated groups, which validates that p21 expression is linked to direct p53 activation. Similar expression of ZsGreen1 across the different groups (Ad-p53-CC, Ad-wt-p53, and Ad-ZsGreen1) in the right column of Figure 5A indicates comparable intratumoral expression of our viral constructs. In addition, p53 immunohistochemistry staining was performed and equal levels of total (i.e. endogenous and exogenous) p53 expression were detected across all groups, including the untreated group, which relates to the known presence of endogenous p53 in MDA-MB-468 cells (data not shown). Figures 5 B and C represent semi-quantitative histoscore analyses of tumor necrosis and p21 up-regulation in the excised tumors from all groups.

Tissues from additional organs (liver, kidney, spleen, heart, and lungs) harvested from animals of all treatment groups showed normal physiology and no abnormalities or signs of pathology (data not shown). However, metastases of tumor cells to the gastrointestinal region were noted in two out of six mice in the Ad-ZsGreen1 group and three out of six mice in the untreated group (data not shown). This may imply an anti-metastatic function of p53-CC as well as wt-p53 in this tumor model although further examination is necessary.

Detection of pathway-specific markers for cell cycle arrest and apoptosis

Based on our observations, we postulate that p53-CC is capable of causing tumor size reduction *in vivo* by favoring the apoptotic pathway, while wt-p53 activity is biased towards inducing cell cycle arrest. To further investigate this hypothesis, we carried out immunoblotting of cleaved (activated) caspase-3 and p21 on samples from *in vitro* and *in vivo*. It is well known that all apoptotic pathways converge on caspase-3 (the main executioner caspase),[35, 36] whereas p21 induction by p53 causes cells to undergo cell cycle G_1 phase arrest.[37–39] Therefore, detection of activated caspase-3 and p21 are acceptable biomarkers for apoptosis and cell cycle arrest, respectively. Figure 6A shows a representative western blot analyses of p21 (middle band) and caspase-3 (bottom band) of MDA-MB-468 cells *in vitro*. MDA-MB-468 cells treated with Ad-p53-CC express lower levels of p21 compared to cells treated with Ad-wt-p53 (Figure 6B), a clear indication of a cell cycle arrest activity of wt-p53. However, higher levels of activated caspase-3 are detected in cells treated with Ad-p53-CC compared to Ad-wt-p53 (Figure 6C, a hallmark of apoptosis induction).

Part of the excised tumor tissues from each animal was homogenized and lysed for western blotting. Figure 6D shows representative western blotting of MDA-MB-468 *in vivo* tumor tissue lysates. Similar to the findings obtained from *in vitro* western blotting (Figures 6A–C), tumor tissues from the Ad-p53-CC treatment group showed lower p21 expression (Figure 6E) but higher caspase-3 induction (Figure 6F).

To further validate our hypothesis about the differential ability of p53-CC and wt-p53 to induce p21-depndent cell cycle arrest, we carried out cell cycle arrest evaluation via DNA content analysis (Figure 7A–C) in MDA-MB-468 cells. Indeed, our data suggest that wt-p53 is capable of causing higher levels of cell cycle arrest at the G0/G1 phase compared to p53-CC ($p < 0.01$) (Figure 7, compare B to A, respectively). Hence, results from Figures 6 & 7 corroborate our hypothesis that p53-CC favors induction of apoptosis *in vitro* and *in vivo*, while wt-p53 is biased towards inducing cell cycle arrest in MDA-MB-468 cells.

DISCUSSION

The data obtained in this report supports our hypothesis that chimeric p53-CC has superior tumor suppressor function compared to wt-p53 *in vitro* and *in vivo* using a dominant negative mutant p53 model. Although the concept of a “superactive” p53 was reported in 2010,[40] there are no known reports of constructing a p53 capable of bypassing the dominant negative effect of mutant p53 in cancer cells and increases apoptosis (over wt-p53). p53-CC induces higher levels of cell death *in vitro* compared to wt-p53 in the 7-AAD assay (Figure 2) as well as in the apoptosis assays: TMRE, caspase-3/7, and annexin-V (Figure 3). To

validate if the superior activity of p53-CC *in vitro* translates *in vivo*, we carried out animal studies using an orthotopic MDA-MB-468 xenograft breast cancer model in mouse mammary fat pads. Indeed, intratumoral injections with Ad-p53-CC achieved substantial tumor regression that is statistically significant compared to the Ad-wt-p53, Ad-ZsGreen1, and untreated groups (Figure 4C), without any sign of treatment toxicity (Figure 4D). H&E staining of tumor tissues revealed higher levels of necrosis in all tumor tissues from mice injected with Ad-p53-CC compared to the Ad-wt-p53, Ad-ZsGreen1, or untreated groups. To test if the observed tumor suppressor activity of p53-CC *in vivo* is p53-dependent, immunohistochemistry staining of p21, the most well studied p53 target gene,[34] was conducted. As expected, p21-positive staining was observed only in the Ad-p53-CC and Ad-wt-p53 treatment groups (Figure 5A) with higher p21 staining with Ad-wt-p53 treatment.

Since p53-CC was able to induce apoptosis (including caspase 3/7), and wt-p53 increased p21 expression, we explored a possible differential mechanism of p53-CC (favoring apoptosis) and wt-p53 (favoring cell cycle arrest) in MDA-MB-468 cells. To test this premise, immunoblotting was carried out on samples from *in vitro* (Figures 6A–C) and *in vivo* (Figures 6D–F) to detect expression levels of p21, which induces cell cycle arrest, and caspase-3, a major executer of apoptosis. Figure 6 revealed that tumor tissues treated with Ad-p53-CC expressed low levels of p21 (reduced cell cycle arrest) but high levels of active caspase-3 (increased apoptosis). In contrast, tumor tissues injected with Ad-wt-p53 expressed high levels of p21 (increased cell cycle arrest) but low levels of caspase-3 (decreased apoptosis).

While Figure 3A–C validated that p53-CC induces higher levels of apoptosis compared to wt-p53, our cell cycle arrest analysis (Figure 7A–C) revealed that wt-p53 induced higher levels of G0/G1 cell cycle arrest compared to p53-CC. These results may provide evidence that p53-CC and wt-p53 may have different mechanism of activity in the MDA-MB-468 breast cancer model.

The transdominant mutant p53 found endogenously in MDA-MB-468 cells retains the ability to hetero-oligomerize with exogenous wt-p53, since its tetramerization domain remains intact.[10] We and others have shown previously that upon hetero-oligomer formation, the activity of exogenous wt-p53 is impaired due to the dominant negative effect of mutant p53 in cancer cells.[12–14] Our chimeric p53-CC was designed to overcome this barrier with a use of an alternative oligomerization domain, a coiled-coil from Bcr (CC). This CC is known to tetramerize as an antiparallel dimer of dimers, similar to the tetramerization domain of wt-p53.[12, 41]

The use of this alternative oligomerization domain allows p53-CC to escape any possible hetero-oligomerization with mutant p53 and consequent transdominant inhibition. Indeed, our previous work validated the ability of p53-CC to exclusively form homo-oligomers. From a gene therapy point of view, the ability of p53-CC to evade transdominant inhibition gives it an advantage over wt-p53 in dominant mutant p53 cancer cells such as MDA-MB-468.

Our viral-mediated gene therapy *in vivo* studies show that p53-CC has superior tumor suppressor activity compared to wt-p53 in the MDA-MB-468 aggressive p53-dominant negative breast cancer model. In fact, p53-CC was capable of achieving significant tumor *regression*, while wt-p53 is only capable of halting tumor *progression* (Figure 4C). Upon further investigation, we discovered that the difference in outcome of the tumor size reduction was due to the ability of p53-CC to activate the apoptotic pathway, whereas wt-p53 activates cell cycle arrest via p21 induction (Figure 8). These findings are supported by western blot analyses from *in vitro* (Figure 6A–C) and *in vivo* (Figure 6D–F) MDA-MB-468 cells/tumors, as well as cell cycle arrest analysis (Figure 7A–C).

Analysis of p53-regulated gene expression patterns may possibly offer an explanation for differential pathway activation between p53-CC and wt-p53 (apoptosis vs cell cycle arrest). It has been shown that p53-responsive gene expression patterns are highly variable, depending on the p53 protein levels in the cell.[42] It is also known that higher levels of active p53 lead to activation of apoptotic genes, while lower levels of p53 activate cell cycle regulator genes.[43] In cells treated with p53-CC vs wt-p53, higher levels of the chimeric p53-CC protein exist compared to levels of active wt-p53 protein in cells (although they have similar expression levels), due to the ability of p53-CC to escape sequestration by mutant p53. Unlike p53-CC, substantial amounts of the wt-p53 protein are forced into inactive hetero-oligomers with endogenous mutant p53 (the dominant negative effect). This reduction in ‘available’ active wt-p53 could lead to failure in binding promoters of apoptotic genes that require higher active p53 protein levels in the cell. Cell cycle regulator genes, such as p21, would be activated instead, since wt-p53 possess higher binding affinities to these promoters (i.e. requires less p53 to bind and activate). In contrast, abundance in active chimeric p53-CC protein levels is found in cells treated with p53-CC (due to escaping transdominant inactivation and not difference in expression levels), which would lead to binding and activation of apoptotic genes promoters. The variability of pathway activation (i.e. p53-CC, apoptosis vs wt-p53, cell cycle arrest) may be specific to this tumor model due to the dominant negative mutant p53 endogenously found in MDA-MB-468 cells/tumors. This is because we have shown previously[12] that p53-CC and wt-p53 induce similar levels of apoptosis in four different non-p53-dominant negative breast cancer cell lines with varying endogenous p53 statuses (H1373 cells: p53 null, HeLa cells: wt-p53, T47D cells: wt-p53 mislocalized, and MDA-MB-231 cells: mutant p53).[12] Furthermore, qRT-PCR analyses and western blotting showed that p53-CC and wt-p53 induced similar levels of p21 gene expression in T47D breast carcinoma cells.

In summary, we have shown for the first time, use of a version of p53 that overcomes the limitations of using wt-p53 for gene therapy. A chimeric superactive p53 has been described as the ‘ultimate cancer therapeutic’.[44] Our p53-CC demonstrates comparable functional transcriptional activity to wt p53,[12] shows significantly improved apoptosis (Figures 2 and 3), and successfully circumvents the dominant negative inactivating effect of endogenous mutant p53 *in vitro*.[12] Importantly, our compelling *in vivo* data (Figure 4) demonstrates that p53-CC is more effective than wt p53, and may serve as a more potent and reliable novel anticancer therapeutic.

MATERIALS AND METHODS

Recombinant Adenovirus Production

Replication-deficient recombinant adenovirus serotype 5 (Ad) constructs were generated using the Adeno-X® Adenoviral Expression System 3 (Clontech, Mountain View, CA) As we have done before.[12] Either wt-p53 or p53-CC was inserted into a cassette under the control of the CMV promoter. A separate CMV promoter controls the expression of ZsGreen1 fluorescent protein for visualization. The empty virus (vector) was used as a negative control. Wt-p53 and p53-CC were PCR amplified with primers containing 15 base pair homology with a linearized pAdenoX vector (Clontech) based on an In-Fusion® HD Cloning Kit (Clontech). Stellar® competent cells (Clontech) were transformed with the adenoviral vector plasmids containing our constructs. Viral DNA was then purified, linearized and transfected into HEK293 cells for packaging and amplification. Viral particles were isolated from HEK293 cells by freeze-thawing, purified using Adeno-X® Mega Purification Kit (Clontech), and dialyzed against storage and proper tonicity buffer (2.5% glycerol (w/v), 25 mM NaCl, and 20 mM Tris-HCl, pH 7.4). The viral titer was determined using flow cytometry per the manufacturer's recommendation.

Cell Lines and Viral Transductions

HEK293 human embryonic kidney cells (ATCC, Manassas, VA) were used for viral production and MDA-MB-468 human breast adenocarcinoma cells (ATCC) harboring a dominant negative mutant p53 were grown as monolayers in DMEM (Invitrogen, Carlsbad, CA) supplemented with 10% fetal bovine serum, 1% penicillin-streptomycin-glutamine, and 0.1% gentamicin. MDA-MB-468 cells were also supplemented with 1% MEM non-essential amino acids (Invitrogen). All cells were incubated in 5% CO_2 at 37°C. The cells were seeded at a density of 3.0×10^5 cells in 6-well plates (Greiner Bio-One, Monroe, NC). Viral transductions were carried out immediately after seeding the cells at multiplicity of infection (MOI) of 200.

7-AAD Assay

Following manufacturer's instructions and as previously described,[45] MDA-MB-468 cells were stained with 7-aminoactinomycin D (7-AAD, Invitrogen) 48 h after transfection. Cells were analyzed and gated for ZsGreen1 (with same fluorescence intensity to ensure equal expression of proteins) using the FACSCanto-II (BD-BioSciences, University of Utah Core Facility) and FACSDiva software. Excitation was set at 488 nm and detected at 507 nm and 780 nm for ZsGreen1 and 7-AAD, respectively. The means from three separate experiments (n=3) were analyzed using one-way ANOVA with Bonferroni's post hoc test.

TMRE Assay

MDA-MB-468 cells were incubated with 100 nM tetramethylrhodamine ethyl ester (TMRE) (Invitrogen) for 30 min at 37 °C 36 h after infection.[46] The time point was determined to be 36 h as a result of several optimization pilot studies for the TMRE assay, and since mitochondrial outer membrane permeabilization occurs prior to caspase-3/7, annexin-V, and 7-AAD detection (48 h). MDA-MB-468 cells were pelleted and resuspended in 300 μL of

annexin-V binding buffer (Invitrogen). Only ZsGreen1 positive cells were analyzed by using the FACS Canto-II (BD BioSciences, University of Utah Core Facility) with FACS Diva software. ZsGreen1 was excited with the 488 nm laser with emission filter 530/35, and TMRE was excited with the 561 nm laser with the emission filter 585/15. Mitochondrial depolarization (loss in TMRE intensity) correlates with an increase in MOMP.[18] Independent transfections of each construct were tested three times (n = 3).

Caspase-3/7 Assay

MDA-MB-468 cells were probed 48 h after treatment using FLICA® 660 Caspase-3/7 Assay Kit (Immunochemistry Technologies, Bloomington, MN). Cells were pelleted, resuspended in 300 μL of 1× wash buffer (Immunochemistry Technologies), and incubated with FLICA® 660 Caspase-3/7 reagent for 45 min per the manufacturer's recommendations. Only ZsGreen1 positive cells were analyzed using the FACS Canto-II (BD BioSciences, University of Utah Core Facility) with FACS Diva software. ZsGreen1 and FLICA® 660 were excited with the 488 nm (emission filter 530/35) and the 635 laser (emission filter 670/30), respectively. Independent transfections of each construct were tested three times (n = 3).

Annexin-V Assay

The annexin-V assay was performed as before.[12, 45] Briefly, 48 h post infection, MDA-MB-468 cells were suspended in 400 μl annexin binding buffer (Invitrogen) and incubated with 5 μl annexin-APC (annexin-V conjugated to allophycocyanin, Invitrogen) for 15 minutes. The incubated cells were ZsGreen1 gated and analyzed using FACSCanto-II. ZsGreen1 and APC were excited at 488 nm and 635 nm wavelengths and detected at 507 nm and 660 nm, respectively. Each construct was tested three times (n=3) and analyzed using one-way ANOVA with Bonferroni's post hoc test.[45]

In Vivo Study

The experimental protocol was approved by the Institutional Animal Care and Use Committee (IACUC) at the University of Utah. All experiments were performed in Female nu/nu athymic mice (6–8 weeks old, Jackson Laboratories, Bar Harbor, ME). Human MDA-MB-468 cells (1×10^7 cells/mouse in 100 μl of serum-free RPMI-1640 medium) were injected subcutaneously into the mammary fat pad located in the right inguinal area. When tumors reached a mean size of 50mm^3, animals were randomized into 4 treatment groups and received single peritumoral injections of adenoviral constructs (5.0×10^8 pfu) in a 50 μl volume prepared fresh on days 0–4 and 7–11. Twenty four hours after the last injection the mice were sacrificed and the tumors as well as the organs were harvested for analyses. Tumor volumes were measured daily using Vernier calipers along the longest width (W) and the corresponding perpendicular length (L). The tumor volume was calculated using V= (L × W (0.5W)). All procedures were performed according to established NIH guidlines and University of Utah Institutional Animal Care and Use Committee approved protocols.

Histology

Animal tumor tissue samples and organs were fixed in 10% formalin for 24 h followed by tissue preparation and embedded in paraffin. Embedded tissues were then sectioned to cut at 4 μm thick sections and mounted on plus slides. Slides from each tumor tissue from all mice in the three treatment groups as well as the untreated group were stained using hematoxylin and eosin and p21 immunohistochemistry stain. Tissue and histological slide preparation was conducted in collaboration with ARUP Laboratories (Salt Lake City, Utah).[47]

Western Blotting

In vivo: fresh tumor tissue samples from animals of each treatment group were collected, snap-frozen in liquid nitrogen, ground with mortar and pestle, re-suspended in 200 mL lysis buffer (62.5 mM Tris-HCl, 2% w/v SDS, 10% glycerol, 1 % protease inhibitor) followed by sonication on ice. Recovered tissue lysates were then centrifuged for 45 min at 14,000 rpm and the supernatants were used for immunoblotting. Standard western blotting procedures[12, 48] were followed using primary antibodies to detect p21/WAF1, cleaved caspase-3, and actin as a loading control. The primary antibodies anti-p21 (ab16767, Abcam, Cambridge, MA), anti-cleaved caspase-3 (#9665P, Cell Signaling Technology, Danvers, MA), anti-actin (mouse, ab3280, Abcam), and anti-actin (rabbit, ab1801, Abcam) were detected with anti-rabbit (#7074S, Cell Signaling Technology) or anti-mouse (ab6814, Abcam) HRP-conjugated antibodies before the addition of SuperSignal West Pico chemiluminescent substrate (Thermo Scientific, Waltham, MA). Signals were detected using a FluorChem FC2 imager and software (Alpha Innotech, Sanata Clara, CA). All experiments were conducted in triplicates.

In vitro: 24 h following infection of MDA-MB-468 cells, 3×10^5 cells were pelleted and resuspended in 200 μL lysis buffer (62.5 mM Tris-HCl, 2% w/v SDS, 10% glycerol, 1 % protease inhibitor), sonicated on ice, and centrifuged for 15 min at 14,000 rpm. The supernatants were used for immunoblotting as described above and densitometry analysis was performed as described before.[49]

Cell Cycle Arrest

The cell cycle arrest analysis was carried out as previously described.[48] Briefly, 1×10^6 MDA-MB-468 cells were infected as described above (Cell Lines and Viral Transductions). Thirty six hours post-infection, cells were collected, washed in PBS (Invitrogen), and fixed in 70% cold ethanol at −20°C for 1 h. Fixed cells were then washed three times with PBS and suspended in a staining solution containing 10 % v/v of 0.5 mg/mL propidium iodide (Sigma-Aldrich, St. Louis, MO), 5% v/v of PBS, 84 % v/v of 4mM Citrate Buffer (Sigma-Aldrich), 0.62 %v/v of RNase A (Sigma-Aldrich), 1% v/v of Triton X-100 (Sigma-Aldrich), and 3% m/v of PEG 6000 (Fluka, St. Louis, MO) for 20 min at 37°C in the dark. An equal volume of salt solution containing 5% of propidium iodide, 1% of Triton X-100, 89% v/v of 0.4M NaCl (Thermo Fisher Scientific Inc, Pittsburgh, PA), and 3% m/v of PEG 6000 was added to the stained cells and incubated at 4°C for 1 h in the dark. Cells were gated at similar intensity level of ZsGreen1. ZsGreen1 and PI were excited at 488 nm and detected at 507 nm and 670 nm, respectively. The means from three separate experiments (n=3) were analyzed using one-way ANOVA with Bonferroni's post hoc test.

Statistical Analysis

One-way ANOVA with Bonferroni's post test was used to compare the different treatment groups and controls. A value of $p < 0.05$ was considered statistically significant. Error bars represent standard deviations from at least three independent experiments (n = 3) except for the animal study (n=6).

ACKNOWLEDGEMENTS

The authors acknowledge the use of DNA/Peptide Core and Flow Cytometry Core (NCI Cancer Center Support Grant P30 CA042014, Huntsman Cancer Institute). Research reported in this publication was supported by the National Cancer Institute of the National Institutes of Health under award number R01-CA151847. We would like to thank Sheryl Tripp (ARUP Laboratories), Ben Bruno, and Geoff Miller for scientific discussions.

REFERENCES

1. Gu W, Roeder RG. Activation of p53 Sequence-Specific DNA Binding by Acetylation of the p53 C-Terminal Domain. Cell. 1997; 90(4):595–606. [PubMed: 9288740]
2. Vogelstein B, Kinzler KW. p53 function and dysfunction. Cell. 1992; 70(4):523–526. [PubMed: 1505019]
3. Vogelstein B, Lane D, Levine AJ. Surfing the p53 network. Nature. 2000; 408(6810):307–310. [PubMed: 11099028]
4. Levine AJ, Momand J, Finlay CA. The p53 tumour suppressor gene. Nature. 1991; 351(6326):453–456. [PubMed: 2046748]
5. Moll UM, Riou G, Levine AJ. Two distinct mechanisms alter p53 in breast cancer: mutation and nuclear exclusion. PNAS. 1992; 89(15):7262–7266. [PubMed: 1353891]
6. Kussie PH, Gorina S, Marechal V, Elenbaas B, Moreau J, Levine AJ, et al. Structure of the MDM2 oncoprotein bound to the p53 tumor suppressor transactivation domain. Science. 1996; 274(5289): 948–953. [PubMed: 8875929]
7. Okal, A.; Reaz, S.; Lim, C. Cancer Biology: Some Causes for a Variety of Different Diseases. In: Bae, YH.; Mrsny, RJ.; Park, K., editors. Cancer Targeted Drug Delivery. New York: Springer; 2013. p. 121-159.
8. Waterman MJ, Waterman JL, Halazonetis TD. An engineered four-stranded coiled coil substitutes for the tetramerization domain of wild-type p53 and alleviates transdominant inhibition by tumor-derived p53 mutants. Cancer Res. 1996; 56(1):158–163. [PubMed: 8548757]
9. Willis A, Jung EJ, Wakefield T, Chen X. Mutant p53 exerts a dominant negative effect by preventing wild-type p53 from binding to the promoter of its target genes. Oncogene. 2004; 23(13): 2330–2338. [PubMed: 14743206]
10. Chan WM, Siu WY, Lau A, Poon RY. How many mutant p53 molecules are needed to inactivate a tetramer? Molecular and Cellular Biology. 2004; 24(8):3536–3551. [PubMed: 15060172]
11. Zeimet AG, Marth C. Why did p53 gene therapy fail in ovarian cancer? The Lancet Oncology. 2003; 4(7):415–422. [PubMed: 12850192]
12. Okal A, Mossalam M, Matissek KJ, Dixon AS, Moos PJ, Lim CS. A Chimeric p53 Evades Mutant p53 Transdominant Inhibition in Cancer Cells. Mol Pharm. 2013; 10(10):3922–3933. [PubMed: 23964676]
13. Junk DJ, Vrba L, Watts GS, Oshiro MM, Martinez JD, Futscher BW. Different mutant/wild-type p53 combinations cause a spectrum of increased invasive potential in nonmalignant immortalized human mammary epithelial cells. Neoplasia. 2008; 10(5):450–461. [PubMed: 18472962]
14. Lim LY, Vidnovic N, Ellisen LW, Leong CO. Mutant p53 mediates survival of breast cancer cells. British Journal of Cancer. 2009; 101(9):1606–1612. [PubMed: 19773755]
15. Okal A, Cornillie S, Matissek SJ, Matissek KJ, Cheatham TE 3rd, Lim CS. Re-Engineered p53 Chimera with Enhanced Homo-Oligomerization That Maintains Tumor Suppressor Activity. Mol Pharm. 2014

16. Schmid I, Krall WJ, Uittenbogaart CH, Braun J, Giorgi JV. Dead cell discrimination with 7-amino-actinomycin D in combination with dual color immunofluorescence in single laser flow cytometry. Cytometry. 1992; 13(2):204–208. [PubMed: 1547670]
17. Serrano MJ, Sanchez-Rovira P, Algarra I, Jaen A, Lozano A, Gaforio JJ. Evaluation of a gemcitabine-doxorubicin-paclitaxel combination schedule through flow cytometry assessment of apoptosis extent induced in human breast cancer cell lines. Japanese journal of cancer research : Gann. 2002; 93(5):559–566. [PubMed: 12036452]
18. Matissek KJ, Mossalam M, Okal A, Lim CS. The DNA binding domain of p53 is sufficient to trigger a potent apoptotic response at the mitochondria. Mol Pharm. 2013; 10(10):3592–3602. [PubMed: 23968395]
19. O'Reilly CM, Fogarty KE, Drummond RM, Tuft RA, Walsh JV Jr. Quantitative analysis of spontaneous mitochondrial depolarizations. Biophys J. 2003; 85(5):3350–3357. [PubMed: 14581236]
20. Ricci JE, Gottlieb RA, Green DR. Caspase-mediated loss of mitochondrial function and generation of reactive oxygen species during apoptosis. J Cell Biol. 2003; 160(1):65–75. [PubMed: 12515825]
21. Chipuk JE, Green DR. How do BCL-2 proteins induce mitochondrial outer membrane permeabilization? Trends in Cell Biology. 2008; 18(4):157–164. [PubMed: 18314333]
22. Mossalam M, Matissek KJ, Okal A, Constance JE, Lim CS. Direct Induction of Apoptosis Using an Optimal Mitochondrially Targeted p53. Mol Pharm. 2012; 9(5):1449–1458. [PubMed: 22380534]
23. Slee EA, Adrain C, Martin SJ. Executioner caspase-3, -6, and -7 perform distinct, non-redundant roles during the demolition phase of apoptosis. The Journal of biological chemistry. 2001; 276(10):7320–7326. [PubMed: 11058599]
24. Lakhani SA, Masud A, Kuida K, Porter GA Jr, Booth CJ, Mehal WZ, et al. Caspases 3 and 7: key mediators of mitochondrial events of apoptosis. Science. 2006; 311(5762):847–851. [PubMed: 16469926]
25. Koopman G, Reutelingsperger CP, Kuijten GA, Keehnen RM, Pals ST, van Oers MH. Annexin V for flow cytometric detection of phosphatidylserine expression on B cells undergoing apoptosis. Blood. 1994; 84(5):1415–1420. [PubMed: 8068938]
26. Vermes I, Haanen C, Steffens-Nakken H, Reutelingsperger C. A novel assay for apoptosis. Flow cytometric detection of phosphatidylserine expression on early apoptotic cells using fluorescein labelled Annexin V. J Immunol Methods. 1995; 184(1):39–51. [PubMed: 7622868]
27. Metzger-Filho O, Tutt A, de Azambuja E, Saini KS, Viale G, Loi S, et al. Dissecting the heterogeneity of triple-negative breast cancer. J Clin Oncol. 2012; 30(15):1879–1887. [PubMed: 22454417]
28. Price R, Gustafson J, Greish K, Cappello J, McGill L, Ghandehari H. Comparison of silk-elastinlike protein polymer hydrogel and poloxamer in matrix-mediated gene delivery. Int J Pharm. 2012; 427(1):97–104. [PubMed: 21982738]
29. Killion J, Radinsky R, Fidler I. Orthotopic Models are Necessary to Predict Therapy of Transplantable Tumors in Mice. Cancer and Metastasis Reviews. 1998; 17(3):279–284. [PubMed: 10352881]
30. Bibby MC. Orthotopic models of cancer for preclinical drug evaluation: advantages and disadvantages. Eur J Cancer. 2004; 40(6):852–857. [PubMed: 15120041]
31. Vantyghem S, Allan A, Postenka C, Al-Katib W, Keeney M, Tuck A, et al. A New Model for Lymphatic Metastasis: Development of a Variant of the MDA-MB-468 Human Breast Cancer Cell Line that Aggressively Metastasizes to Lymph Nodes. Clin Exp Metastasis. 2005; 22(4):351–361. [PubMed: 16170671]
32. Garlich JR, De P, Dey N, Su JD, Peng X, Miller A, et al. A vascular targeted pan phosphoinositide 3-kinase inhibitor prodrug, SF1126, with antitumor and antiangiogenic activity. Cancer Research. 2008; 68(1):206–215. [PubMed: 18172313]
33. Nielsen LL, Lipari P, Dell J, Gurnani M, Hajian G. Adenovirus-mediated p53 gene therapy and paclitaxel have synergistic efficacy in models of human head and neck, ovarian, prostate, and

breast cancer. Clinical cancer research : an official journal of the American Association for Cancer Research. 1998; 4(4):835–846. [PubMed: 9563876]

34. Laptenko O, Beckerman R, Freulich E, Prives C. p53 binding to nucleosomes within the p21 promoter in vivo leads to nucleosome loss and transcriptional activation. Proceedings of the National Academy of Sciences of the United States of America. 2011; 108(26):10385–10390. [PubMed: 21606339]
35. Tait SW, Green DR. Mitochondria and cell death: outer membrane permeabilization and beyond. Nature reviews. Molecular cell biology. 2010; 11(9):621–632. [PubMed: 20683470]
36. Fulda S, Debatin KM. Extrinsic versus intrinsic apoptosis pathways in anticancer chemotherapy. Oncogene. 2006; 25(34):4798–4811. [PubMed: 16892092]
37. el-Deiry WS, Harper JW, O'Connor PM, Velculescu VE, Canman CE, Jackman J, et al. WAF1/CIP1 is induced in p53-mediated G1 arrest and apoptosis. Cancer Research. 1994; 54(5):1169–1174. [PubMed: 8118801]
38. Waldman T, Kinzler KW, Vogelstein B. p21 is necessary for the p53-mediated G1 arrest in human cancer cells. Cancer Research. 1995; 55(22):5187–5190. [PubMed: 7585571]
39. Waldman T, Zhang Y, Dillehay L, Yu J, Kinzler K, Vogelstein B, et al. Cell-cycle arrest versus cell death in cancer therapy. Nature medicine. 1997; 3(9):1034–1036.
40. Lane DP, Cheok CF, Lain S. p53-based cancer therapy. Cold Spring Harb Perspect Biol. 2010; 2(9):a001222. [PubMed: 20463003]
41. Wichmann C, Becker Y, Chen-Wichmann L, Vogel V, Vojtkova A, Herglotz J, et al. Dimer-tetramer transition controls RUNX1/ETO leukemogenic activity. Blood. 2010; 116(4):603–613. [PubMed: 20430957]
42. Yamada T, Hiraoka Y, Ikehata M, Kimbara K, Avner BS, Das Gupta TK, et al. Apoptosis or growth arrest: Modulation of tumor suppressor p53's specificity by bacterial redox protein azurin. Proceedings of the National Academy of Sciences of the United States of America. 2004; 101(14):4770–4775. [PubMed: 15044691]
43. Chen X, Ko LJ, Jayaraman L, Prives C. p53 levels, functional domains, and DNA damage determine the extent of the apoptotic response of tumor cells. Genes & development. 1996; 10(19):2438–2451. [PubMed: 8843196]
44. Lane DP, Cheok CF, Lain S. p53-based cancer therapy. Cold Spring Harb Perspect Biol. 2010; 2(9):a001222. [PubMed: 20463003]
45. Mossalam M, Matissek KJ, Okal A, Constance JE, Lim CS. Direct induction of apoptosis using an optimal mitochondrially targeted p53. Mol. Pharm. 2012; 9(5):1449–1458. [PubMed: 22380534]
46. Krohn AJ, Wahlbrink T, Prehn JH. Mitochondrial depolarization is not required for neuronal apoptosis. The Journal of neuroscience : the official journal of the Society for Neuroscience. 1999; 19(17):7394–7404. [PubMed: 10460246]
47. Salama ME, Rajan Mariappan M, Inamdar K, Tripp SR, Perkins SL. The value of CD23 expression as an additional marker in distinguishing mediastinal (thymic) large B-cell lymphoma from Hodgkin lymphoma. Int J Surg Pathol. 2010; 18(2):121–128. [PubMed: 19223373]
48. Reaz S, Mossalam M, Okal A, Lim CS. A Single Mutant, A276S of p53, Turns the Switch to Apoptosis. Mol Pharm. 2013
49. Woessner DW, Lim CS. Disrupting BCR-ABL in combination with secondary leukemia-specific pathways in CML cells leads to enhanced apoptosis and decreased proliferation. Mol Pharm. 2013; 10(1):270–277. [PubMed: 23211037]

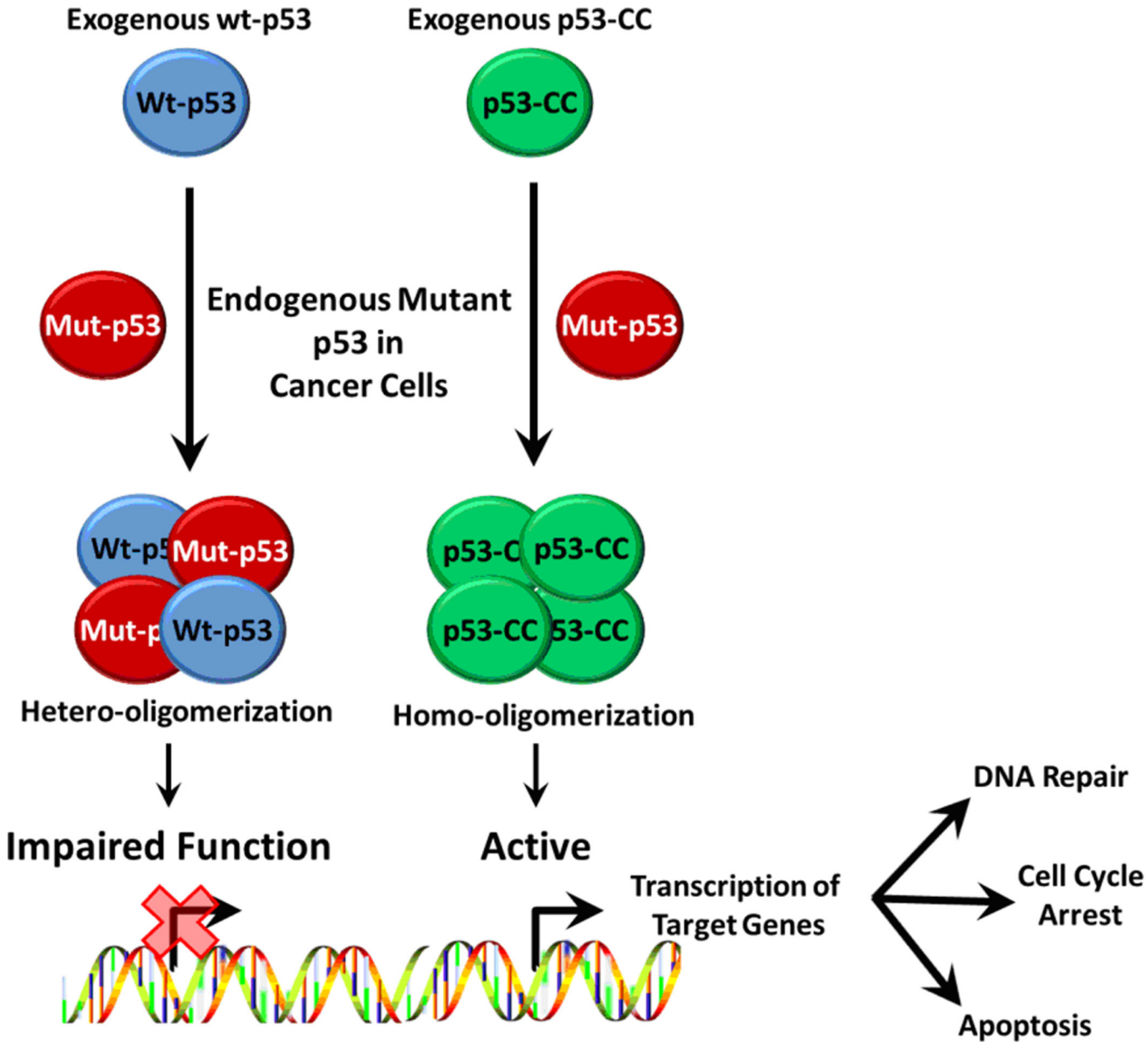

Figure 1.

Schematic representation of the fates of wt-p53 (left) and p53-CC (right) in the presence of endogenous mutant p53 in cancer cells. Wt-p53 (left) is sequestered into hetero-oligomers that have an impaired transcription function, while p53-CC (right) can exclusively form homo-oligomers that retain full tumor suppressor activity.

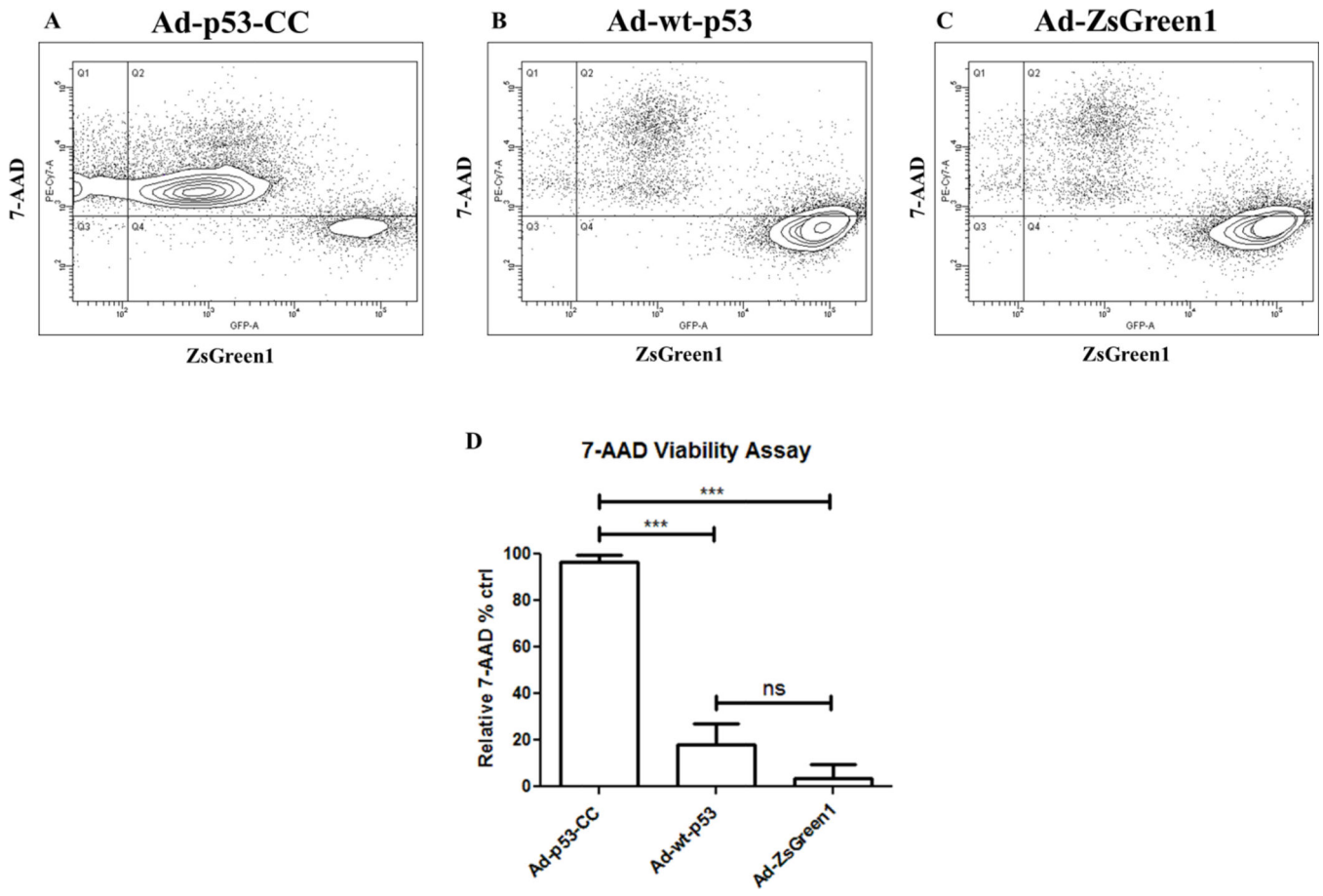

Figure 2.

7-AAD staining of apoptotic and necrotic was performed. 48 h after viral transfection, cells were analyzed and gated for ZsGreen1. (A–C) Representative individual contour plots from each transfection and treatment group showing only ZsGreen1-gated cells. Q1&Q2= 7-AAD positive cells; Q3&Q4= 7-AAD negative cells. (D) Percentage of cell death induced by each transfection and treatment group. Mean values were analyzed using one-way ANOVA with Bonferroni's post test; ns= non-significant, *** $p < 0.001$. Error bars represent standard deviations from at least three independent experiments (n = 3).

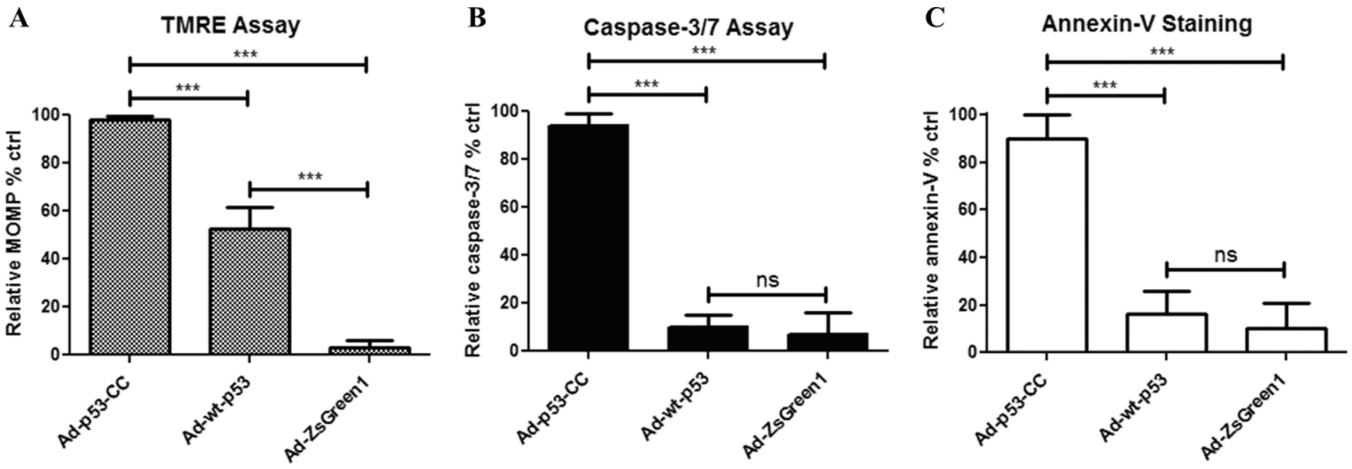

Figure 3.

Induction of apoptosis is measured by (A) TMRE, (B) Caspas-3/7, and (C) Annexin-V. In all three assays, MDA-MB-468 cells trated with Ad-p53-CC undergo higher levels of apoptosis compared to cells infected with Ad-wt-p53 or the negative control Ad-ZsGreen1. Mean values were analyzed using one-way ANOVA with Bonferroni's post test; ns= non-significant, *** $p < 0.001$. Error bars represent standard deviations from at least three independent experiments (n = 3).

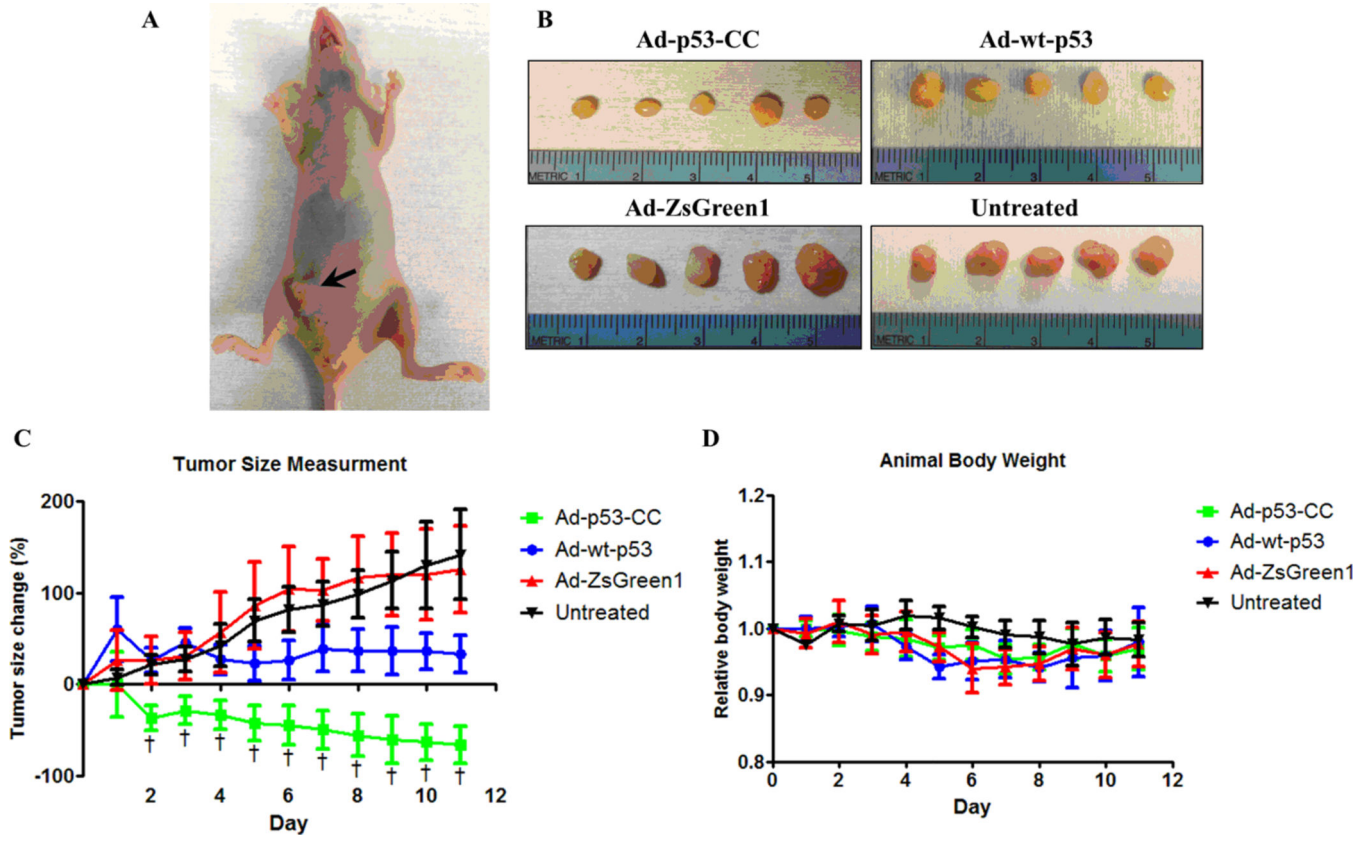

Figure 4.

Effect of viral gene therapy using p53-CC and wt-p53 on induced the aggressive p53-dominant negative MDA-MB-468 human breast adenocarcinoma in female athymic nu/nu mice. (A) A representative image of a mouse in the study. For tumor inductions, MDA-MB-468 cells were injected in the right mammary fat pad of the inguinal area (highlighted by the black arrow). (B) Representative images of the excised tumors from each treatment group scaled to the same ratios. (C) Tumor size measured with calipers daily and normalized to Day 0. (D) Animal weights as measured daily and normalized relative to weights from Day 0. Six mice per group were used for this study. Mean values were analyzed using one-way ANOVA with Bonferroni's post test; †$p < 0.001$. Error bars represent standard deviations.

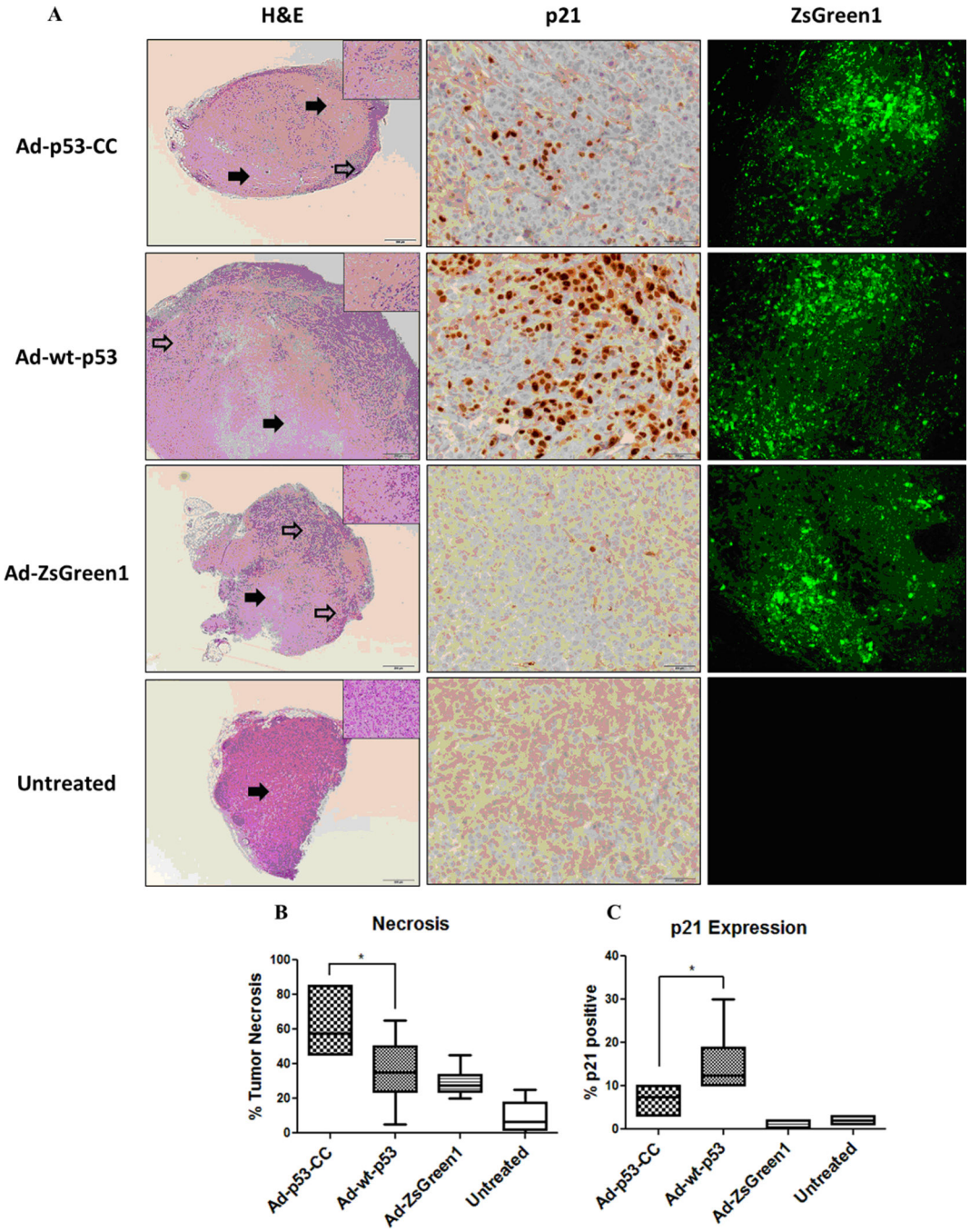

Figure 5.

Representative photomicrographs showing the effects of the different treatment groups on tumor tissues visualized via H&E staining (A) left column, p21 immunohistochemistry staining (A) middle column, and ZsGreen1 fluorescence (A) right column. (A)Solid black arrows (left column) indicate necrotic cells, while open arrows indicate non-necrotic areas. 3,3' diaminobenzidine (DAP) stains the nuclei of p21-positive cells brown (middle column). Examination of the H&E staining microscopically revealed higher levels of necrosis in all tumor tissues from mice injected with Ad-p53-CC compared to the Ad-wt-p53, Ad-

ZsGreen1, or untreated groups. p21 immunohistochemistry staining revealed higher levels of p21 induction in the Ad-wt-p53 treatment group compared to the Ad-p53-CC treatment group. Semi-quantitative histoscore analyses of (B) tumor necrosis and (C) p21 up-regulation in the excised tumors from all groups is shown. Mean values were analyzed using one-way ANOVA with Bonferroni's post test; * $p < 0.05$. Error bars represent standard deviations (n=6).

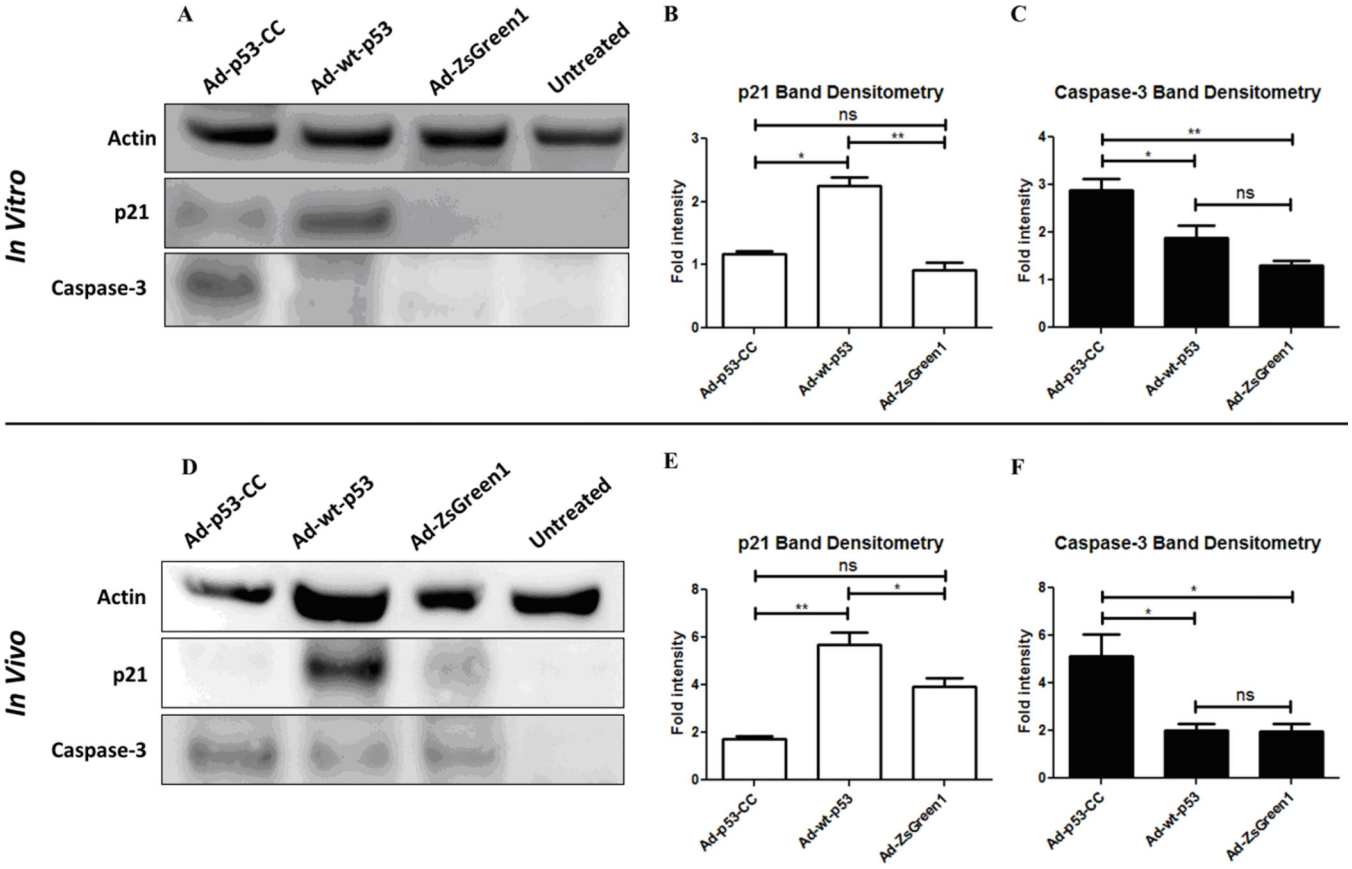

Figure 6.

Representative cropped western blots of MDA-MB-468 (A–C) *in vitro* cell lysates and (D–F) homogenized tumors from the *in vivo* study treated with Ad-p53-CC, Ad-wt-p53, Ad-ZsGreen1, or untreated. Western analyses show that MDA-MB-468 cells (A) and tumor tissues (D) treated with Ad-p53-CC both express lower levels of p21, but higher levels of activated caspase-3 compared to cells treated with Ad-wt-p53. No significant levels of p21 or caspase-3 induction were observed in cells (A) or tumors (D) injected with Ad-ZsGreen1 or untreated. Semi-quantitative densitometric analyses was carried out as described before[49] to evaluate p21 (B) and caspase-3 (C) expression *in vitro* as well as expression of p21 (E) and caspase-3 (F) expression *in vivo* normalized (fold intensity) to the p21 and cleaved caspase-3 endogenous levels in untreated samples. Mean values were analyzed using one-way ANOVA with Bonferroni's post test; * $p < 0.05$, ** $p < 0.01$, and *** $p < 0.001$. Error bars represent standard deviations (n=3).

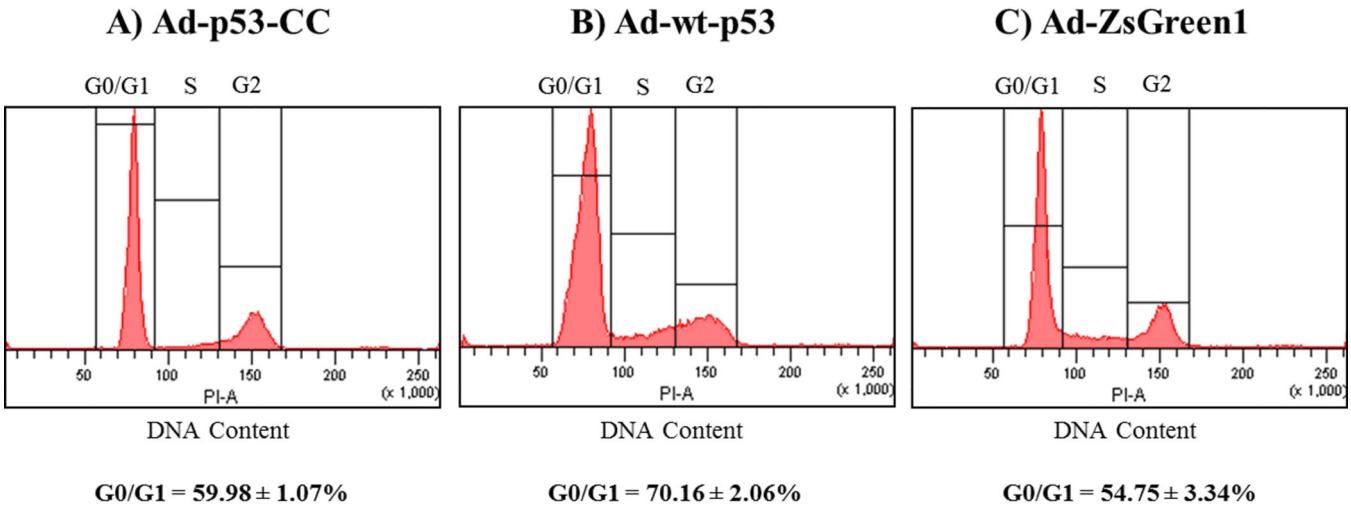

Figure 7.

Representative histograms of cell cycle arrest analysis 36 h post-infection in MDA-MB-468 cells. The values reported are averaged DNA content ± SD of infected cells with A) Ad-p53-CC, B) Ad-wt-p53, and C) Ad-ZsGreen1 in G0/G1 phase from three different experiments (n=3). Statistical analysis was performed using one-way ANOVA with Bonferroni's post test.

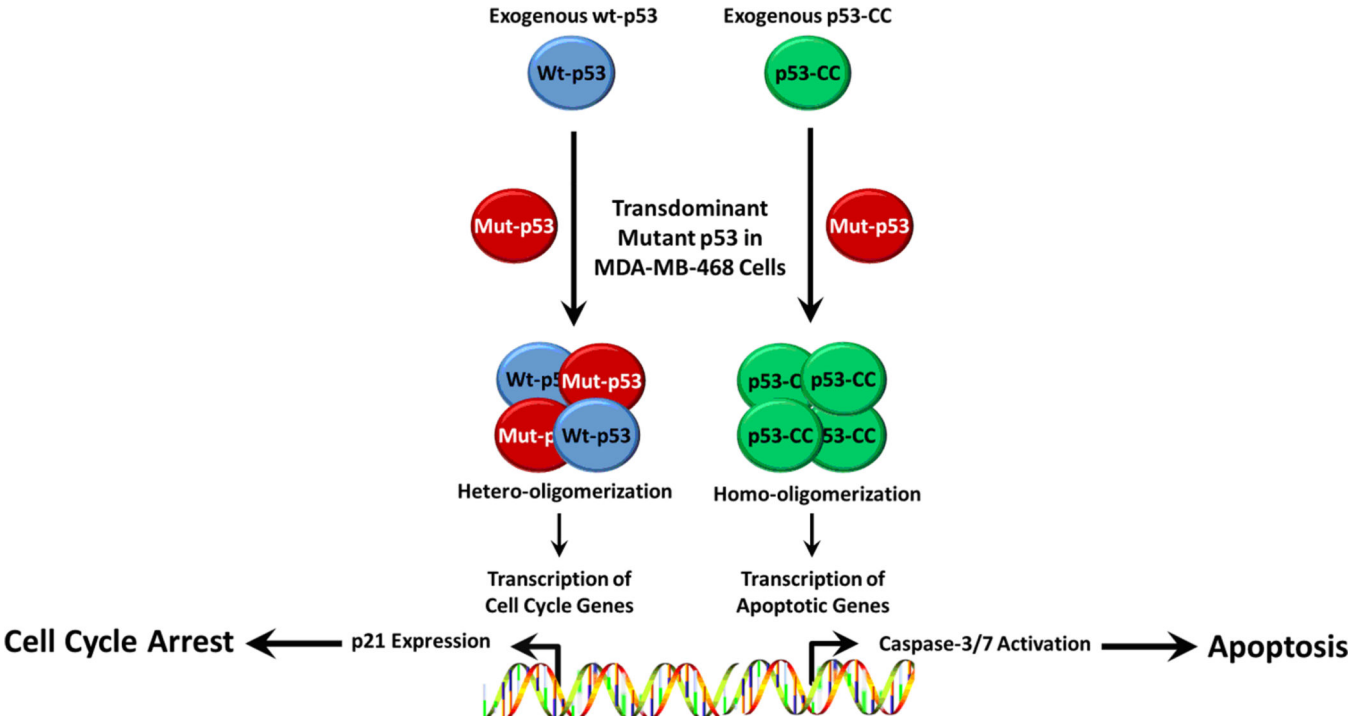

Figure 8.

Schematic representation of the outcomes of wt-p53 (left) and p53-CC (right) activation. Wt-p53 induces cell cycle arrest via p21 expression (left), while p53-CC induces cell death via the apoptotic pathway (right).